

Composite Polymer Electrolyte based on Liquid Crystalline Copolymer with High-temperature Stability and Bendability for All-solid-state Lithium-ion Batteries

Xiaoyan Cao, Jiaming Cheng, Xiubo Zhang, Dan Zhou, Yongfen Tong*

School of Environmental and Chemical Engineering, Nanchang Hangkong University, 696 Fenghe South Avenue, Nanchang 330063, China

*E-mail: tongyongfen@nchu.edu.cn

Received: 16 September 2019 / Accepted: 2 November 2019 / Published: 30 November 2019

In this study, a novel composite polymer electrolyte consist of 8-arm block liquid crystalline copolymer (8-PEG-MALC), 8-arm poly(ethylene glycol) (8-PEG), polyethylene (glycol) diacrylate (PEGDA) and bistrifluoromethanesulfonimide lithium salt (LiTFSI) was prepared successfully. The branching 8-PEG ensure high ionic conductivity of the all solid state polymer, crosslinking agent PEGDA endow good mechanical property, and 8-arm block liquid crystalline copolymer with a birefringent mesogens to tune the morphology of the composite polymer electrolytes. The polymer electrolytes can form a transparent and flexible film with nanoscale microphase separation structure, which creating well-defined ion conducting channels. The electrochemical properties of composite polymer electrolytes are analyzed and the highest ionic conductivity reaches $6.2 \times 10^{-5} \text{ S cm}^{-1}$ at room temperature after annealed from fixed temperature. It also displays high temperature stability up to 150°C , which is higher than traditional electrolytes. More intriguingly, the assembled $\text{LiFePO}_4/\text{Li}$ cells using the composite polymer electrolytes exhibit good charge/discharge cycles at 95°C . The good electrochemical properties, temperature stability and bendability of the composite polymer electrolytes indicate it potentially as a very promising material for all-solid-state flexible lithium ion batteries.

Keywords: self-assemble; composite polymer electrolytes; bendability; lithium-ion batteries

1. INTRODUCTION

Lithium-ion batteries have been widely applied in our daily life as energy storage devices owing to their high energy density and efficiency during the last two decades[1-3]. To satisfy the demand of various shaped electronic devices, flexible and bendable lithium-ion batteries with unique features is growing rapidly as one of promising candidates as power power sources[4-6]. Due to the leakage, flammability and poor chemical stability of the organic liquid electrolytes, the solid-state polymer electrolytes are ideal candidates for deformable lithium ion batteries because it has great

advantages of electrochemical stability window, high mechanical stability, flexibility and safety[7-9]. PEO have been considered as the most effective polymer for solid state polymer electrolyte because of its solvability of lithium ions[10-12]. However, owing to the high crystallinity of PEO, the ionic conductivity of PEO-based electrolytes show relatively low (10^{-8} to 10^{-6} S cm^{-1}) at room temperature[13, 14]. Consequently, it is critical issue to improve the ion conductivity based on PEO-based electrolyte. Extensive studies have been focus on introducing branching, cross-linking and copolymer structures or incorporating some other copolymer aim to enhance ion mobility and improve ion conductivity without sacrificing the mechanical properties. [15-18]

As a special material, liquid crystalline structure can be introduced to polymer electrolytes for electrochemical devices because they can construct ion-conductive pathways by self-assembly[19-23]. Many studies also pay attention to use block copolymer for polymer electrolytes because it not only enhanced polymer electrolytes ion conductivity but also enhanced the mechanical strength[24-26]. Thus, the PEO-based block copolymers with liquid-crystalline properties have been exploited as electrolytes, which can transport ions efficiently by formation of nanoscale ion pathway[27-30].

Herein, we report a novel liquid crystalline copolymer composite polymer electrolyte consisting of 8-arm block liquid crystalline copolymers (8-PEG-MALC), 8-arm PEG and polyethylene (glycol) diacrylate (PEGDA). The PEGDA is used as cross-linker and supporting framework to enhance the mechanical strength. The 8-arm block liquid crystalline copolymers as filler to blend with 8-arm PEG matrix. Self-assemble ability of liquid crystalline block copolymer would induce microphase separation and create well-defined ion conducting channels to enhance ionic conductivity[31]. The composite polymer electrolytes include different weight ratios 8-arm block liquid crystalline copolymers (8-PEG-MALC) with bistrifluoromethanesulfonimide lithium salt (LiTFSI) as doping salts have been successfully prepared. It was expected to enhance ionic conductivity which forms wide and highly mobile 2D ion-conductive pathway (Fig. 1).

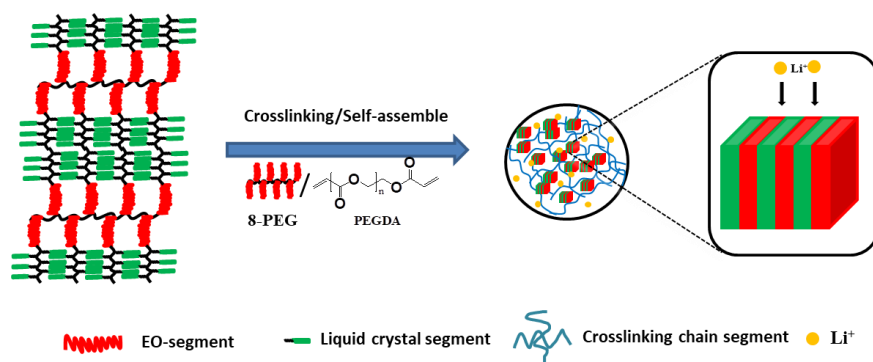


Figure 1. Schematic illustration of crosslinking and self-assembly of liquid crystalline copolymer composite polymer electrolyte.

Meanwhile, the composite polymer electrolytes display good thermal stability and high bendability.

2. EXPERIMENTAL SECTION

2.1 Synthesis of copolymer and characterization of the membranes

All the experiments details and characterization methods are described in the Supporting Information (SI). The synthetic routes for the target 8-arm block liquid crystalline copolymer (8-PEG-MALC) are shown in Scheme S1. The copolymers were prepared through a simple ATRP method and the synthesis steps are similar with our previous work.[32] The M_n of the 8-arm block liquid crystalline copolymer is about 41361 by gel permeation chromatography (GPC). The structures of the intermediates and the copolymers are confirmed by FT-IR (Fig. S1a and S2) and ^1H NMR (Fig. S1b). Both FT-IR and ^1H NMR prove that the 8-arm copolymer with mesogens was synthesized successfully.

3. RESULT AND DISCUSSION

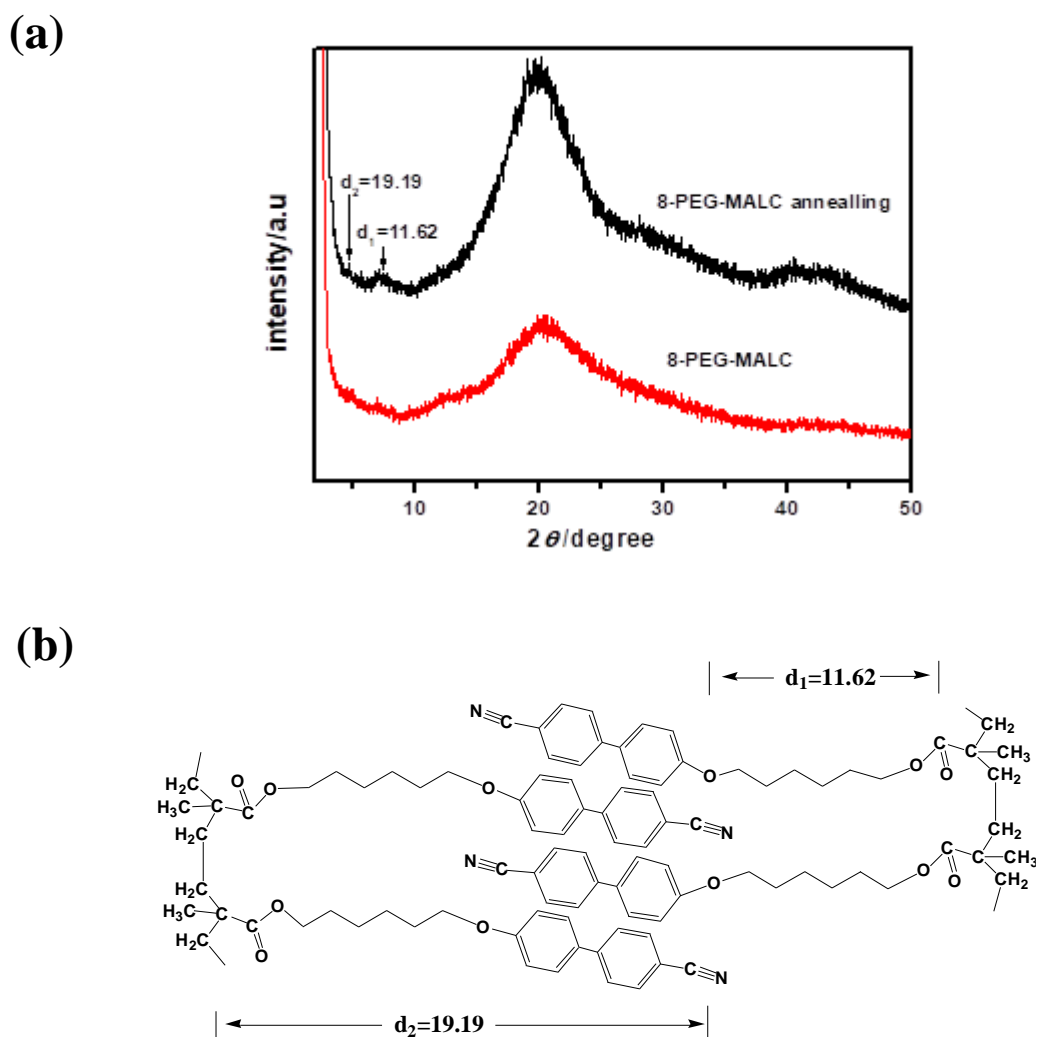


Figure 2. (a) XRD pattern of 8-PEG-MALC as-cast and annealing film. (b) Proposed bilayer packing arrangement of 8-PEG-MALC.

Composite polymer electrolytes were achieved by casting the mixed acetonitrile solution on a plate and polymerizing under UV-light. The composite polymer electrolytes including different ratios 8-PEG-MALC, 8-PEG, PEGDA and bistrifluoromethanesulfonimide lithium salt (LiTFSI) as doping salts had been successfully prepared. The composite electrolytes are classified by the weight ratio of each component $m(8\text{-PEG}) : m(\text{PEGDA}) = 1.5 : 1$, weight ratios of 8-PEG-MALC are 0, 10%, 20%, 30%, 40%, respectively and $[\text{EO}]:[\text{Li}^+]=16$, as shown in Table 1. As an example, the sample 8-PEG-MALC-30 with weight ratio of 8-PEG-MALC was 30%.

The X-ray diffraction of the liquid crystalline block copolymer is provided in Fig. 2a. The X-ray diffraction pattern of 8-PEG-MALC showed a broad peak about 20° , may be attributed to PEG segment crystallization. Compared with the as-cast film of 8-PEG-MALC, the XRD diffractogram of the film annealed at the liquid crystalline state show an obvious reflection at $2\theta=7.59^\circ$, corresponding to the spacing of 11.62\AA , which represents the local ordered arrangement of the polymer.

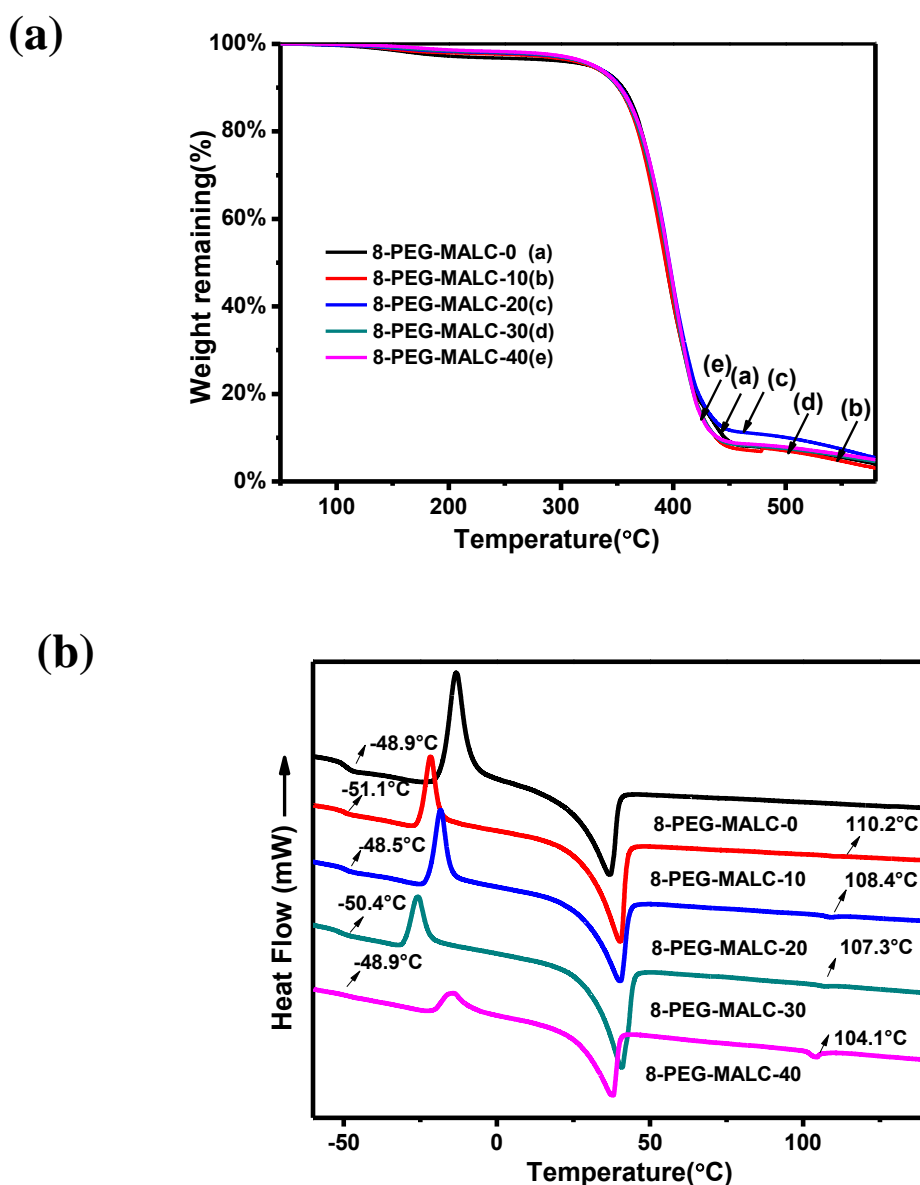


Figure 3. (a) TG curves and (b) DSC thermograms of composite polymer electrolyte recorded under nitrogen atmosphere during the second heating scans at a scan rate of $10^\circ\text{C min}^{-1}$.

The peak located at $2\theta = 4.6^\circ$ ($d_2=19.19 \text{ \AA}$) is associated to the distance between the backbone to cyanobiphenyl mesogenic, that is, the methylene chain distance of the side chain, suggesting the formation of a bilayered structure (Fig. 2b). The results show that the bilayer packing arrangement of 8-PEG-MALC can be informed via orientation after thermal annealing. The XRD pattern of composite polymer electrolytes with different component are also studied (Fig. S3). The decreased intensity of two reflections at $2\theta = 19.2$ and 23.4° with the increase of 8-PEG-MALC, means that introducing in mesogen-containing 8-PEG-MALC can suppress the tendency of PEG to crystallize.

For the solid polymer electrolyte, Thermal stability is important parameter for application in lithium-ion batteries. Fig. 3 summarizes the TG curves and DSC thermograms of composite polymer electrolyte in nitrogen flows. As shown in Fig. 3a, the different composite polymer electrolytes exhibit similar thermal behaviors and the weight-loss step appear between 350°C and 450°C , which suggest that all the samples decompose above 350°C in one step. And only tiny amounts of residues at 500°C is remained, the corresponding residue amounts of 8-PEG-MALC-0, 8-PEG-MALC-10, 8-PEG-MALC-20, 8-PEG-MALC-30, 8-PEG-MALC-40 are around 7.8%, 7.7%, 10.8%, 8.0%, 8.2%, respectively. The results show that composite polymer electrolyte possesses high-temperature tolerance and stability. The DSC traces from the 2nd heating scans of copolymer 8-PEG-MALC shows two peaks at 28.5 and 104.1°C in the high temperature range, related to the smectic B- smectic A and smectic A- isotropic state transitions, suggesting the cyanobiphenyl mesogens induces the star copolymers with good liquid crystalline property (Fig. S4). Fig. 3b shows the DSC thermograms of composite polymer electrolytes with various concentrations of 8-PEG-MALC. The composite polymer electrolyte show obviously glass transition temperature between -47.7°C and -51.1°C , which meant that the EO chain is flexible and the composite system show good segmental motion. The LC to isotropic transition temperatures (T_i) are located between 104.1 to 110.2°C and the liquid crystalline phase are more obvious with the increasing amounts of 8-PEG-MALC for the composite polymer electrolytes, indicating that the composite electrolytes possess liquid crystals properties and good assembly ability.

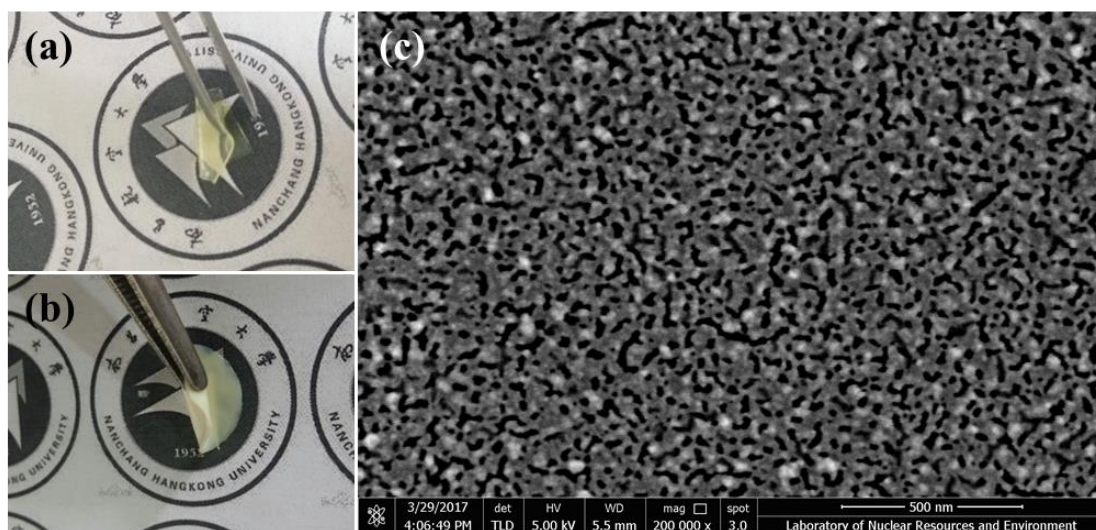


Figure 4. Photos of (a) 8-PEG-MALC-0 and (b) 8-PEG-MALC-30, (c) SEM image of composite polymer electrolytes containing LiTFSI ($[\text{O}]/[\text{Li}] = 16$).

As shown in Fig. 4a and 4b, a flexible and deformable free-standing film composite polymer electrolyte with a thickness of 150-200 μm could be obtained by photo-initiated polymerization. Fig. 4c depicts the surface microstructure of 8-PEG-MALC-30 electrolytes film after the thermal annealing from the fixed temperature. The SEM shows an obvious nanoscale micro-phase separation. It means that cyanobiphenyl mesogens of the block copolymer stack in a regular formation, consequently inducing composite electrolytes to achieve microphase separation morphology, which is consistent with the XRD results. The results show that liquid crystalline block copolymer self-assemble behavior can facilitate the formation of the bilayer packing arrangement by annealing, further to form lithium ions transport channel.

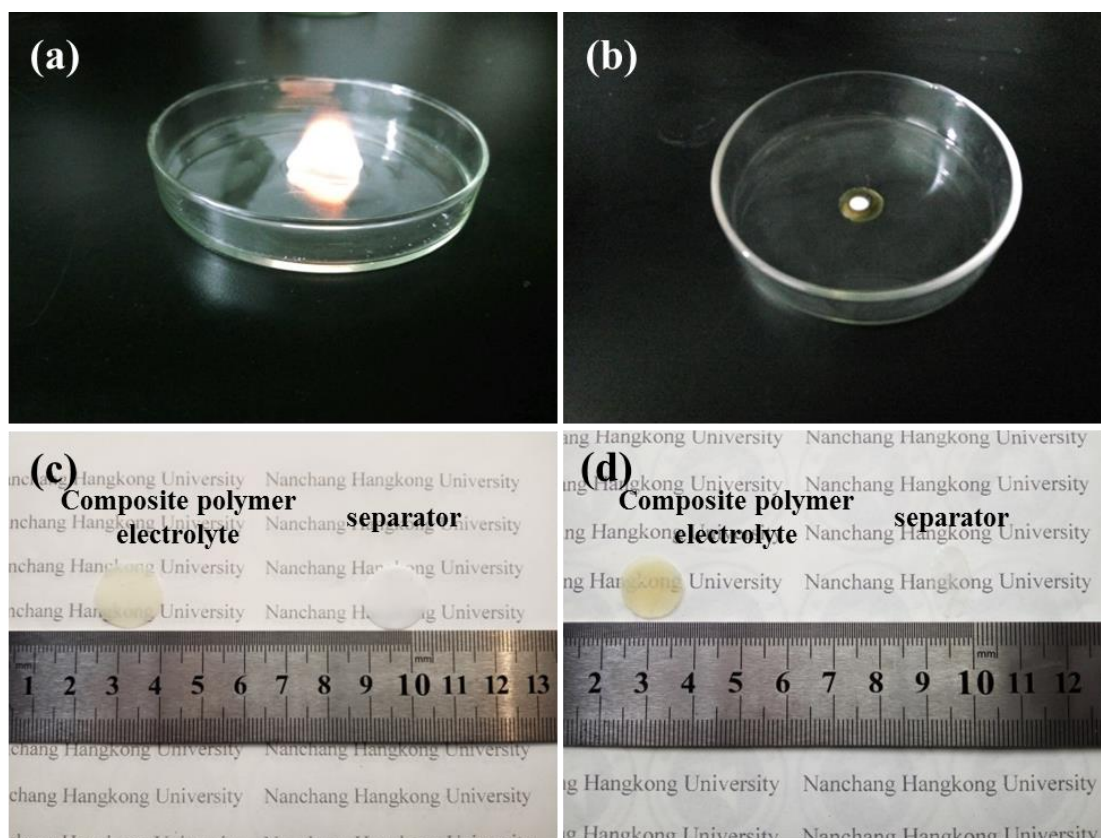


Figure 5. Combustion testing of (a) 1M LiPF_6 in EC/EMC/DMC =1:1:1 and (b) composite polymer electrolytes. Photos of the thermal shrinkage of composite polymer electrolyte and commercial separator (c) before and (d) after exposure to 150 $^\circ\text{C}$ for 60 min.

It is well known that safety issue of electrolyte is very important for lithium-ion battery. However, the liquid electrolyte is easy to cause fire or explosion when the battery is exposed to short circuit, overcharge, or high temperature conditions. Fig. 5 shows combustion testing of 1M LiPF_6 in EC/EMC/DMC =1: 1: 1 and composite polymer electrolytes. Compared with the highly flammable liquid electrolyte (Fig. 5a) and composite polymer electrolyte (Fig. 5b), the latter obviously display low flammability and hardly ignited. In order to further investigate the thermal shrinkage at high temperature for electrolyte, the composite polymer electrolyte and commercial separator were stored at 150 $^\circ\text{C}$ for 60min. Fig. 5c and 5d present the photos of the composite polymer electrolyte and

commercial separator before and after heating. The composite polymer electrolyte display high thermal stability and negligible change in its dimension. However, the commercial separator shows drastic shrinkage at high temperature. Therefore, this remarkable thermal property of composite polymer electrolyte guarantees the safety performance of lithium-ion batteries.

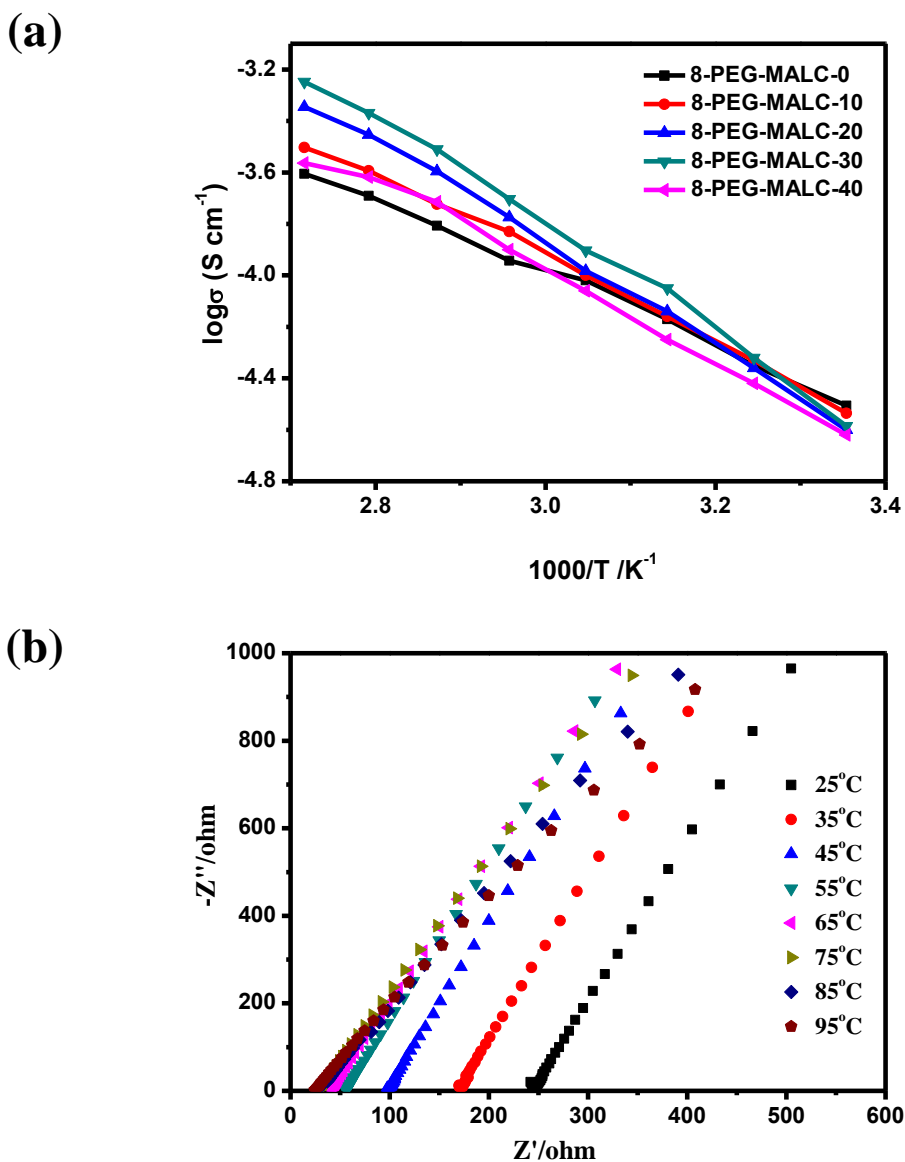


Figure 6. (a) Ionic conductivity of composite polymer electrolyte and (b) Impedance spectra of 8-PEG-MALC-30 at difference temperature, over the frequency range from 10 Hz~1MHz with an amplitude of 10 mV.

To study the ion conductivity of the composite polymer electrolytes, the AC impedance spectroscopy measurement was used to analyze the ionic conductivity of the electrolytes with a SS/CPE/Li cell. Ionic conductivity (σ) was calculated by the equation as follow.

$$\sigma = \frac{d}{A \times R_b} \tag{1}$$

And the d represents the distance between the two electrodes, A is the area of the polymer electrolyte film and R_b is the value of the polymer electrolyte resistance which was obtained from impedance data. As shown in Fig. 6a, with the increasing of temperature, the resistances of the electrolytes become lower and the ionic conductivities become higher.

The different content introduction of 8-PEG-MALC also has a significant effect on the ionic conductivity of composite electrolytes. The 8-PEG-MALC-0 shows the highest ionic conductivity value among all the composite electrolytes at room temperature, while the composite electrolyte with liquid crystalline block copolymer possesses higher ionic conductivity when increase the temperature. The highest conductivity was achieved for 8-PEG-MALC-30 at the elevated temperature. The improvement in the ionic conductivity of the composite polymer electrolytes should be ascribed to the formation of the ordered channel and form highly mobile ion-conductive pathways. The reduced ionic conductivity of 8-PEG-MALC-40 electrolyte film with further increasing the component of 8-arm copolymer is related to the increase non-ion conducting content of cyano-biphenyl segment and the relative higher T_g . So the amount of 8-PEG-MALC is important on the electrochemical performance, and the appropriate amount of the copolymer not only benefits to form better ion transport channel, but also improve the good chain segment mobility of PEG. For the solid state electrolyte system, the ion conductivity value is fitted to the VTF equation,

$$\sigma T^{1/2} = A \exp\left(\frac{-E_a}{R(T-T_0)}\right) \quad (2)$$

where σ is the ionic conductivity value at different temperatures, A is a frequency factor depending on the mobility and number of charge carriers, E_a is the activation energy, R is the perfect gas constant, $8.314 \text{ J K}^{-1} \text{ mol}^{-1}$, and T_0 is the Vogel temperature at which relaxation times become infinite or the mobility of ions goes to zero. According to the literature, T_0 is 50 K below the glass transition temperature of polymer electrolytes based on polyether [10, 33-35]. From the VTF equation, it can be knew that a plot of $\ln(\sigma T^{0.5})$ vs. $1/(T-T_0)$ should be linear, which is exactly observed in Fig. S5. The E_a values for the electrolytes are listed in Table 1. It shows the values between 6.33 and 9.31 kJ mol^{-1} , indicating that the ion movement is largely contributed by the $-\text{EO}_n-$ segment motion.[36]

Table 1. Ionic conductivity of composite polymer electrolyte (at 25°C) as-cast films and annealed from the fixed temperature.

Composite polymer electrolyte	8-PEG : PEGDA (wt%)	8-PEG-MALC (wt%)	LiTFSI [O]/[Li ⁺]	Conductivity As-cast film ($\sigma/\text{S cm}^{-1}$)	Conductivity Annealed ($\sigma/\text{S cm}^{-1}$)	E_a KJ/mol
8-PEG-MALC-0	1.5 : 1	0	16	3.1×10^{-5}	3.1×10^{-5}	6.33
8-PEG-MALC-10	1.5 : 1	10	16	2.9×10^{-5}	4.2×10^{-5}	7.46
8-PEG-MALC-20	1.5 : 1	20	16	2.5×10^{-5}	5.3×10^{-5}	8.64
8-PEG-MALC-30	1.5 : 1	30	16	2.6×10^{-5}	6.2×10^{-5}	9.31
8-PEG-MALC-40	1.5 : 1	40	16	2.4×10^{-5}	3.8×10^{-5}	7.61

The E_a values of the all the electrolytes is from 6.33 to 9.31kJ/mol, indicating that the ionic movement in a polymer electrolyte is greatly contributed by the flexible EO segment.

The impedance spectrums of 8-PEG-MALC-30 at difference temperature from 25°C to 95°C were provided in Fig. 6b. The lower impedance data indicate that the electrolyte has higher conductivity. The ionic conductivity value of as-cast films and annealed from fixed temperature are also presented in Table1. For the 8-PEG-MALC-0 electrolyte, the ionic conductivity value has no obvious change before and after annealing. However, the ionic conductivities of the as-cast and annealed film based on the 8-PEG-MALC-30 are $2.6 \times 10^{-5} \text{ S cm}^{-1}$ and $6.2 \times 10^{-5} \text{ S cm}^{-1}$, respectively. The ionic conductivity value is improved 2.5-fold by annealing, which is attributed to formation of ordered ion transportation pathways upon assembling.

The composite polymer electrolyte demonstrated here is compared with some other polymer electrolytes based on PEO or PEG segment in Table 2. The relative high ionic conductivity value further proves that the orientation of the composite polymer electrolytes is beneficial to the rapid transmission of ions, thus increase the ionic conductivity.

Table 2. Comparison of ionic conductivity of polymer electrolyte based on PEO or PEG reported in the literature.

Composite polymer electrolyte	Temperature (°C)	Ionic conductivity ($\sigma/\text{S cm}^{-1}$)	Reference
8-PEG-MALC-30	25	6.2×10^{-5}	This work
PEGDE-PEGDA-1000	30	5.3×10^{-5}	[12]
PEGDA-DVB	30	2.8×10^{-6}	[15]
PS-PEO-PS	60	2.3×10^{-4}	[16]
xPEO ₁₀	30	3.2×10^{-6}	[17]
POSS-2PEG6k	30	2.1×10^{-5}	[18]
HSLCP	30	5.98×10^{-5}	[23]

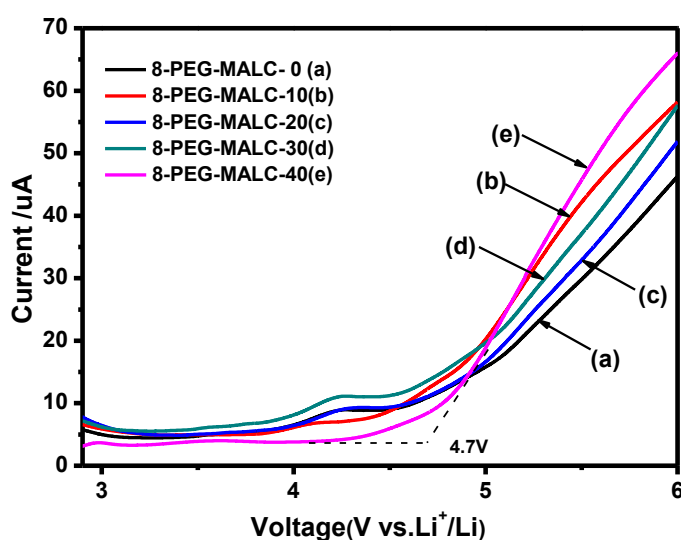


Figure 7. Linear sweep voltammograms of composite polymer electrolyte in a SS/CPE/Li cell at a scan rate of 1.0 mV s^{-1} at room temperature.

Electrochemical stability of composite polymer electrolytes is important for the long service performance of lithium ion batteries. Electrochemical stability window was achieved by linear sweep voltammograms to study the electrochemical stability of composite polymer electrolytes. Fig. 7 shows linear sweep voltammograms of composite polymer electrolytes in the range of 3-6V at a scan rate of 1.0 mV s^{-1} , obtained from the cell Li/CPE/SS. The current began abrupt increase at around 4.5V. The rapid increase of the current is generally known to be the decomposition of the electrolytes.[37-39] It means that all of the composite electrolytes are stable up to 4.5V vs. Li/Li^+ , which could be applied to high voltage polymer lithium-ion battery.

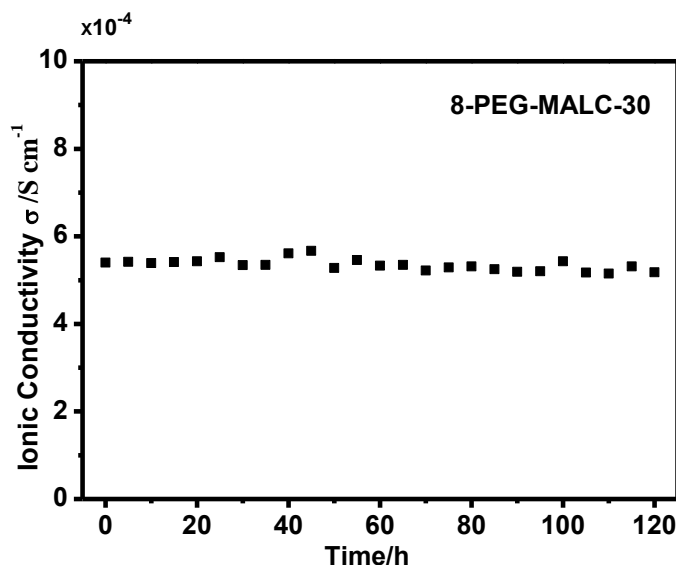


Figure 8. Ionic conductivity of 8-PEG-MALC-30 composite polymer electrolyte vs. time at 95 °C.

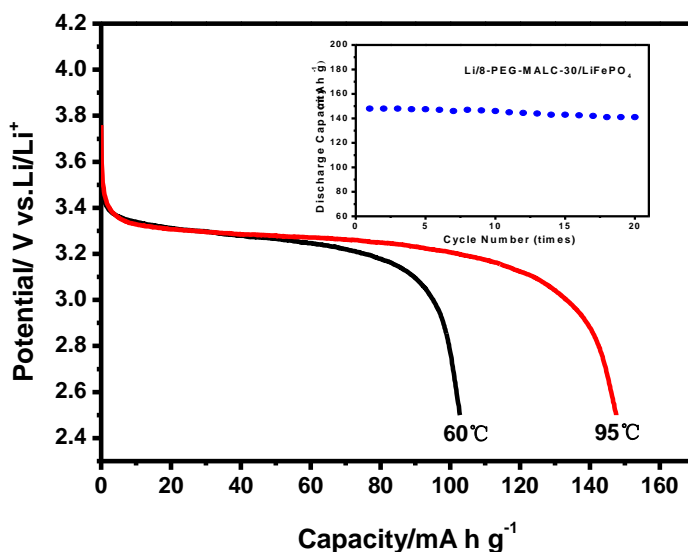


Figure 9. Initial cycle discharge curves of Li/8-PEG-MALC-30/LiFePO₄ cell at a charge/discharge current density of 0.1 C (50°C and 95°C) and cycling properties of Li/8-PEG-MALC-30/LiFePO₄ at 95 °C (0.1C, 2.5-4V).

The ionic conductivity of 8-PEG-MALC-30 composite polymer electrolyte vs. time at 95°C are also probed (Fig. 8). The composite polymer electrolyte maintained the ionic conductivity value around $5.6 \times 10^{-4} \text{ S cm}^{-1}$ for 120h at 95°C. It implies that the composite polymer electrolyte can ensure the long-term application at high-temperature.

The charge-discharge experiments of LiFePO₄/electrolyte/Li coin cell were evaluated by using the composite polymer electrolytes. The cut-off voltage was set at 2.5V for discharge and 4V for charge at 0.1C. Fig. 9 gives initial cycle charge-discharge curves of LiFePO₄/8-PEG-MALC-30/ Li cell at 50°C and 95°C. It is clearly shown that the batteries present discharge capacity of 147.9 mAh g⁻¹ at 95°C and 103.2 mAh g⁻¹ at 50°C, respectively. The discharge capacity at 95°C higher than 50°C, indicate that polymer chain movement easier and more suitable to be operated at high temperature. The cycling properties of Li/8-PEG-MALC-30/LiFePO₄ at 95°C are also shown in Fig. 9 (Inset) . The cell retention value of discharge capacity reaches up to 95.3% after 20 cycles. The stable cycling behaviors indicate that the composite polymer electrolytes can be a promising electrolyte candidate for solid Lithium-ion battery.

4. CONCLUSION

In summary, we have successfully obtained some novel composite polymer electrolytes with liquid crystalline copolymer. The composite polymer electrolytes display nanoscale microphase separation structures by liquid crystalline self-assembly to form ion-conductive pathways. All the polymer electrolytes could be thermally stable up to 350°C and display non-flammability by the combustion testing. The 8-PEG-MALC-30 electrolytes exhibit the highest ionic conductivity value of $6.2 \times 10^{-5} \text{ S cm}^{-1}$ at room temperature and $5.6 \times 10^{-4} \text{ S cm}^{-1}$ at 95°C. Meanwhile, the composite polymer electrolytes display electrochemistry stability at high temperature and show wide electrochemical stability window up to 4.5V. The good ionic transport of the composite polymer electrolytes combine with its improved safety, stability, flexibility, and good electrochemical properties can be used as a potential solid electrolyte. Thus, it facilitates successful development of bendability lithium-ion batteries with good performance and robust safety.

ACKNOWLEDGEMENTS

This work was supported by the National Natural Science Foundation of China (21404054) and Natural Science Foundation of Jiangxi Province (20192BAB206013).

SUPPORTING INFORMATION

1S. Experimental section

1s.1 materials

8-arm poly(ethylene glycol) (8-PEG, Mw = 20000) was bought from Shanghai ToYong Bio-Tech Co. Ltd.. 4'-Cyano-4-hydroxybiphenyl, methacryloyl chloride (97%), anhydrous magnesium sulfate, aluminium oxide, 2-bromoisobutyryl bromide, potassium carbonate, anhydrous triethylamine (>99%), 2-benzoyl-2-propanol, 1,1,4,7,10,10-hexamethyl triethylene tetramine (HMTETA, Elf Atochem), 6-Bromo-1-Hexanol, copper(I) bromide (CuBr, 98%) were purchased from Energy Chemical. lithium bis(trifluoromethane sulfonyl)imide (LiTFSI, 98%) and Poly(ethylene glycol) diacrylate (PEGDA) were purchased from Aldrich. LiFePO₄, carbon black, PVdF binder and lithium metal anode were bought from Damao Chemicals, Tianjin, China. Dichloromethane is distilled from CaH₂ under nitrogen atmosphere prior to use. Tetrahydrofuran, toluene and methylbenzene is distilled from sodium before used. Methanol, ethanol, acetone and ether were purchased from Shanghai Reagent Co., Ltd. Ultrapure deionized (DI) water was used as appropriate.

1s.2 Synthesis of the monomer

Synthesis of 4-cyano-4'-[(6-hydroxyhexyl)oxy]biphenyl

4'-Cyano-4-hydroxybiphenyl (1.95 g, 0.01 mol), potassium carbonate (4.14g, 0.03mol) and acetone (100ml) were added in a round bottom flask with a reflux condenser and a magnetic stirrer. The reaction mixture was heated to 65°C and refluxed for 2-3 h, then added 6-bromo-1-hexanol (2.72 g, 0.015 mol). The reaction mixture was stirred under reflux for 24 h. After cooling, hydrochloric acid (200 ml, 1M) was added and the precipitated product was extracted with chloroform (3 × 100 ml). The chloroform extracts were washed with water and dried by anhydrous MgSO₄. After filtration and evaporation of the solvent with a rotary vapor, the crude product was recrystallized from methanol to yield 2.4 g (73%) of white solid. ¹H NMR (δ_{ppm}, CDCl₃): 1.04–1.93 (m, 8H, -(CH₂)₄-), 3.69(t, 2H, -OCH₂OH-), 4.10(m, PhOCH₂, 2H), 6.89–7.67(m, 8H, aromatic).

Synthesis of monomers 6-[(4-cyano-4'-biphenyl)oxy]hexyl methacrylate (MALC)

4-cyano-4'-[(6-hydroxyhexyl)oxy]biphenyl (2.95 g, 0.01 mol) were dissolved in dry tetrahydrofuran (100ml) in a round bottom flask with a reflux condenser, a nitrogen inlet and a magnetic stirrer. After stirring for 2-3h, anhydrous triethylamine (1.11 g, 0.011 mol) and methacryloyl chlorid (1.05 g, 0.01 mol) was added dropwise. Then, the reaction mixture was stirred for overnight. The white precipitated solid is removed through filtration and evaporation of the solvent with a rotary vapor, the crude product is recrystallized from ethanol to yield 2.54g (70%) of white crystals. ¹H NMR (δ_{ppm}, CDCl₃) : 7.66 (d, 4H), 7.52 (d, 2H), 6.98(d, 2H), 6.09(s, 1H), 5.54(s, 1H), 4.16(t, 2H), 4.01(t, 2H), 1.94(s, 3H), 1.83(q, 2H), 1.74(q, 2H), 1.52(q, 2H), 1.24 (q, 2H).

1s.3 Synthesis of macroinitiator 8-PEG-Br

Under N₂ atmosphere, 2g 8-arm poly(ethylene oxide) was dissolved in dry dichloromethane in a dried 100ml Schlenk flask with a magnetic stirrer. Anhydrous triethylamine (0.82g, 8mmol) and 2-bromoisobutyryl bromide (1.84g, 8mmol) was added drop wise under ice/water bath. Then, the

solution was stirred for 48 h and allowed to reach room temperature slowly. The product is achieved from an excess of ether. Yield 1.8g (85.7). $^1\text{H NMR}$ (δ ppm, CDCl_3): 4.27 (d, 2H), 3.75 (t, 2H), 3.62(m, 272H), 3.54(t, 2H), 3.51(t, 2H), 1.87 (s, 6H).

1s.4 Synthesis of copolymers 8-PEG-MALC by Atom Transfer Radical Polymerization (ATRP)

A dried 100ml Schlenk flask is charged with macroinitiator 8-PEG-Br (0.5g, 0.025mmol), MALC (1.81g, 5mmol), CuBr(28.5g, 0.2mmol), ligand 1,1,4,7,10,10-hexamethyltriethylenetetramine (28.5mg,0.2mmol) and distilled toluene (6ml) under nitrogen. The solution was degassed three times with freeze–pump–thaw cycles. Then the flask was transferred to a thermostated oil bath at 80°C. After 6h of polymerization, the solution was diluted with THF, passed through a column of neutral alumina and precipitated from an excess of ether, filtered, and vacuum dried, got the product of 1.97g.

1s.5 Preparation of composite polymer electrolyte

8-PEG, 8-PEG-MALC, PEGDA, LiTFSI salt and photoinitiator 2-benzoyl-2-propanol are dissolved in acetonitrile and stirred for 24h. The casting solution is put into Teflon dishes, then under UV light for 15S and the solvent is slowly evaporated at room temperature for 24h, the as-prepared films were finally dried under vacuum at 60°C for 24 h. The composite polymer electrolytes are designated by the weight percentage of 8-PEG-MALC (0, 10%, 20%, 30%, 40%), and referred as 8-PEG-MALC-0, 8-PEG-MALC-10, 8-PEG-MALC-20, 8-PEG-MALC-30 and 8-PEG-MALC-40, respectively.

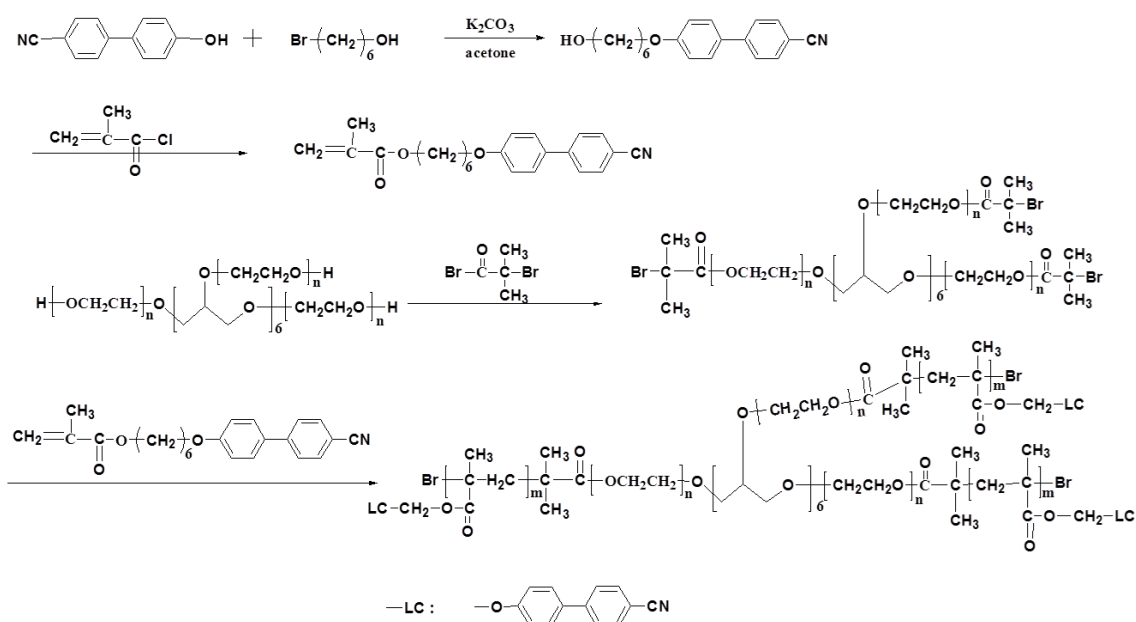
1s.6 Characterization of the membranes

The infrared spectra (IR) were performed on a Shimadzu IR Prestige-21 Fourier transform infrared spectrophotometer on KBr substrates. The structures of the synthesized monomer and copolymer were determined by nuclear magnetic resonance ($^1\text{H NMR}$) spectroscopy on a Bruker ARX 400 NMR spectrometer with tetramethylsilane ($\delta=0$) as the internal standard and DMSO- d_6 as the solvent. The gel permeation chromatography (GPC) is conducted with a Breeze Waters system equipped with a Rheodyne injector, a 1515 Isocratic pump and a Waters 2414 differential refractometer using polystyrenes as the standard and tetrahydrofuran as the eluent at a flow rate of 1.0mL/min. The surface and composite films were investigated via scanning electron microscopy (SEM) using an environmental scanning electron microscope (ESEM, FEI Quanta 200) by the composite membranes were gold-sprayed prior to measurements. Thermogravimetric analysis (TGA) was conducted using a Perkin-Elmer TGA 7 under a nitrogen flow, with the sample size of about 5~10 mg and at the heating rate of 10°C min $^{-1}$. The X-ray diffraction (XRD) tests were determined using a Bruker D8 Focus X-ray diffractometer which were done in the flat-plate $\theta/2\theta$ geometry on a spinner stage and carried out from range of 2°~50° at the room temperature and the scanning rate of 1° min $^{-1}$. The thermal analysis of the polymer electrolyte was obtained by the differential scanning calorimetry (DSC) using a Shimadzu DSC-60 differential scanning calorimeter at the constant heating/cooling rate of 10°C min $^{-1}$. Alternating current (AC) impedance measurements of the composite polymer electrolytes were carried out using a CHI660 electrochemical workstation (CH Instruments) over the frequency range from 10 Hz~1MHz with an amplitude of 10 mV. All the electrolytes were put into

the two stainless steel working electrode, and stainless steel reference and counter electrodes. These were obtained in the temperature range of 20~100°C, and the system was maintained at each selected temperature for at least 1 h to ensure that the electrolyte reached thermal equilibrium. Linear sweep voltammetry (LSV), which was used to studies the electrochemical stability of composites polymer electrolyte, in a SS/CPE/Li cell at the scan rate of 1 mV s⁻¹ over the range from 0 to 8 V (vs. Li/Li⁺) at room temperature. And, as the working electrolytes, SS and lithium metal are reference and counter electrodes, respectively. Also the fabrication of gas-tight test cells was performed on an argon-filled glove box with a moisture level < 0.1 ppm. Assembled the Li/ CPE /LiFePO₄ coin cells were used to the tests of charge-discharge cycling, which were carried out at higher temperature using a Neware battery testing system (model BTS-51, ShenZhen, China). The LiFePO₄ cathode was fabricated with weight percentage of 85% LiFePO₄, 5% polyvinylidene fluoride and 10% acetylene black. Which were stirred in N-methylpyrrolidone to obtain a homogeneous mixture, then deposited on the electrode films and dried at 80°C for 24 h. Coin cells were assembled and sealed in an argon-filled glove box with a moisture level < 0.1 ppm.

2S. Result and Discussion

The 8-arm block liquid crystalline copolymer (8-PEG-MALC) was prepared by atom transfer radical polymerization and the synthesis routes for monomers and 8-arm block liquid crystalline copolymers are shown in scheme S1.



Scheme. S1. Synthesis routes for monomers and 8-arm block liquid crystalline copolymers.

Fig. S1a shows the FT-IR spectra of 8-PEG-Br, MALC and 8-PEG-MALC. The characteristic peaks of MALC are observed at 2230 (—CN—) and 2950 cm⁻¹ (—C=C—). The absorbance peak of —C—O—C— groups at 1108 cm⁻¹ is derived from 8-PEG. Meanwhile, the characteristic absorption peaks of 8-PEG-MALC observed at 2230 cm⁻¹ (—CN—) implies the presence of cyano biphenyl group. The ¹H

NMR spectra of 8-PEG-MALC is presented in Fig. S1b. Obviously, the number of the repeat LC unit is estimated originating from the oxyethylene protons of PEG at 3.62 ppm and the phenyl proton of the LC group at 6.98 ppm. The FT-IR spectra of composite polymer electrolytes with different component are shown in Fig. S2. The 8-PEG-MALC is confirmed by the presence of the stretching vibration band of $-\text{CN}-$ at 2230.

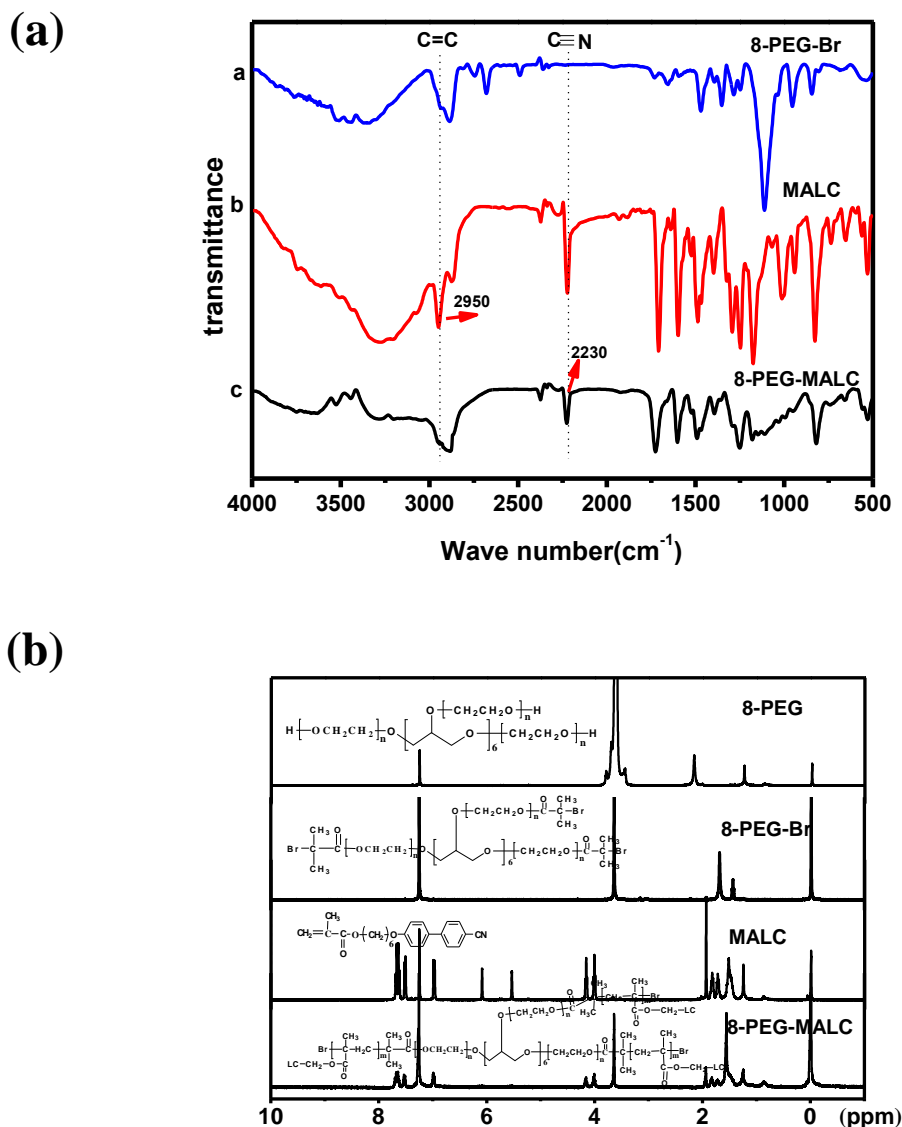


Figure S1. (a) FT-IR spectra of 8-PEG-Br, MALC and 8-PEG-MALC (KBr substrates). (b) ^1H NMR spectra of 8-PEG, 8-PEG-Br, MALC, 8-PEG-MALC with tetramethylsilane ($\delta=0$) as the internal standard and DMSO-d_6 as the solvent.

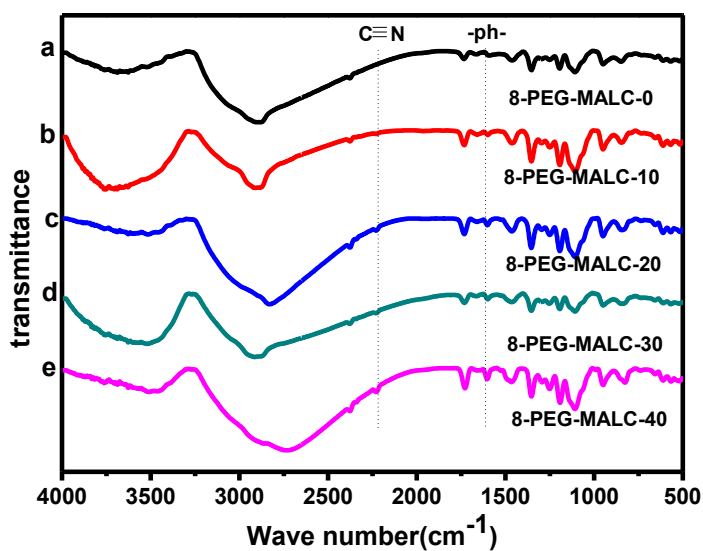


Figure S2. FT-IR spectra of 8-PEG-MALC-0, 8-PEG-MALC-10, 8-PEG-MALC-20, 8-PEG-MALC-30, 8-PEG-MALC-40 (KBr substrates).

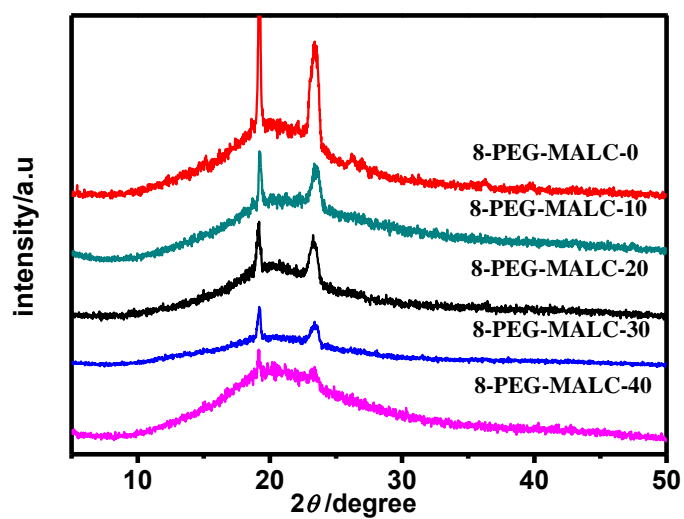


Figure S3. XRD pattern of composite polymer electrolytes carried out from range of $2^\circ \sim 50^\circ$ at the room temperature and the scanning rate of 1°min^{-1} .

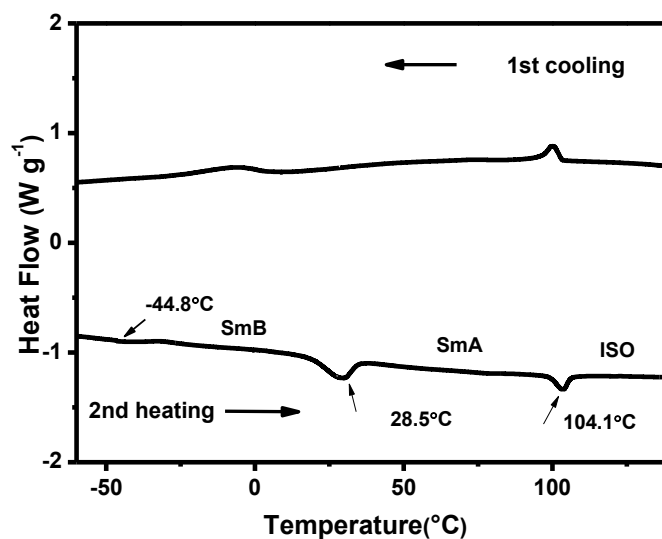


Figure S4. DSC thermograms of 8-PEG-MALC recorded under nitrogen atmosphere during the second heating scans at a scan rate of $10\text{ }^{\circ}\text{C min}^{-1}$. Iso: isotropic; SmA: smectic A; SmB: smectic B.

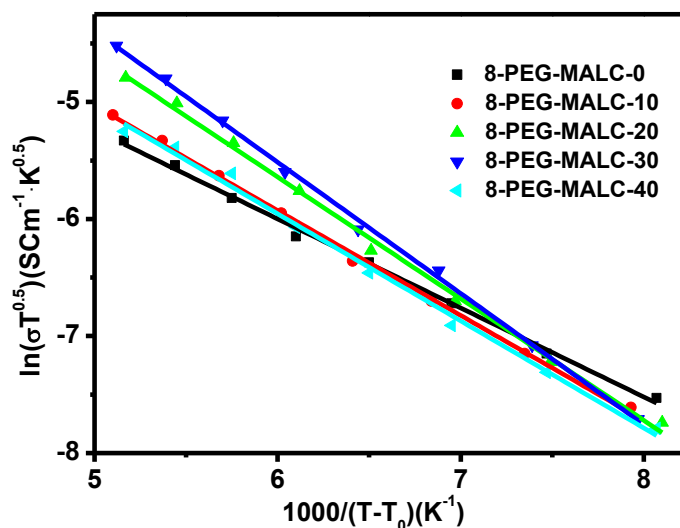


Figure S5. The VTF curves of composite polymer electrolytes based on VTF equation.

References

1. J.-M. Tarascon and M. Armand, *Nature*, 414(2001)359.
2. S. Chu and A. Majumdar, *Nature*, 488(2012)294.
3. W. Xu, J. Wang, F. Ding, X. Chen, E. Nasybulin, Y. Zhang and J.-G. Zhang, *Energy Environ. Sci.*, 7(2014)513.
4. L. Ye, X. Shi, Z. Zhang, J. Liu, X. Jian, M. Waqas and W. He, *Adv. Mater. Interfaces*, (2017)1601236.

5. Y.-H. Li, X.-L. Wu, J.-H. Kim, S. Xin, J. Su, Y. Yan, J.-S. Lee and Y.-G. Guo, *J. Power Sources*, 244(2013)234.
6. K. Lee, S. Kim, J. Park, S. H. Park, A. Coskun, D. S. Jung, W. Cho and J. W. Choi, *J. Electrochem. Soc.*, 164(2017)A2075.
7. M. Que, Y. Tong, G. Wei, K. Yuan, J. Wei, Y. Jiang, H. Zhu and Y. Chen, *J. Mater. Chem. A*, 4(2016)14132.
8. Q. Lu, Y. B. He, Q. Yu, B. Li, Y. V. Kaneti, Y. Yao, F. Kang and Q. H. Yang, *Adv. Mater.*, (2017)1604460.
9. J. Bae, Y. Li, J. Zhang, X. Zhou, F. Zhao, Y. Shi, J. B. Goodenough and G. Yu, *Angew. Chem. Int. Ed.*, 57(2018)2096.
10. L. Porcarelli, C. Gerbaldi, F. Bella and J. R. Nair, *Sci. Rep.*, 6(2016)19892.
11. R. Miao, J. Yang, Z. Xu, J. Wang, Y. Nuli and L. Sun, *Sci. Rep.*, 6(2016)21771.
12. H. Duan, Y.-X. Yin, X.-X. Zeng, J.-Y. Li, J.-L. Shi, Y. Shi, R. Wen, Y.-G. Guo and L.-J. Wan, *Energy Storage Mater.*, 10(2018)85.
13. F. Deng, X. Wang, D. He, J. Hu, C. Gong, Y. S. Ye, X. Xie and Z. Xue, *J. Membr. Sci.*, 491(2015)82.
14. Y. Tong, Y. Xu, D. Chen, Y. Xie, L. Chen, M. Que and Y. Hou, *RSC Adv.*, 7(2017)22728.
15. H. Ben youcef, O. Garcia-Calvo, N. Lago, S. Devaraj and M. Armand, *Electrochim. Acta*, 220(2016)587.
16. R. Bouchet, T. N. T. Phan, E. Beaudoin, D. Devaux, P. Davidson, D. Bertin and R. Denoyel, *Macromolecules*, 47(2014)2659.
17. D. G. Mackanic, W. Michaels, M. Lee, D. Feng, J. Lopez, J. Qin, Y. Cui and Z. Bao, *Adv. Energy Mater.*, 8(2018)1800703.
18. Q. Pan, D. M. Smith, H. Qi, S. Wang and C. Y. Li, *Adv. Mater.*, 27(2015)5995.
19. N. Yamashita, S. Watanabe, K. Nagai, M. Komura, T. Iyoda, K. Aida, Y. Tada and H. Yoshida, *J. Mater. Chem. C*, 3(2015)2837.
20. J. Sakuda, M. Yoshio, T. Ichikawa, H. Ohno and T. Kato, *New J. Chem.*, 39(2015)4471.
21. B. Soberats, E. Uchida, M. Yoshio, J. Kagimoto, H. Ohno and T. Kato, *J. Am. Chem. Soc.*, 136(2014)9552.
22. B. Soberats, M. Yoshio, T. Ichikawa, H. Ohno and T. Kato, *J. Mater. Chem. A*, 3(2015)11232.
23. S. Wang, A. Wang, X. Liu, H. Xu, J. Chen, L. Zhang, *Electrochim. Acta*, 259(2018)213.
24. D. R. Wang, K. H. Wujcik, A. A. Teran and N. P. Balsara, *Macromolecules*, 48(2015)4863.
25. R. Bouchet, S. Maria, R. Meziane, A. Aboulaich, L. Lienafa, J.-P. Bonnet, T. N. Phan, D. Bertin, D. Gigmes and D. Devaux, *nat. mater.*, 12(2013)452.
26. I. Villaluenga, X. C. Chen, D. Devaux, D. T. Hallinan and N. P. Balsara, *Macromolecules*, 48(2015)358.
27. G. Zardalidis, E. F. Ioannou, K. D. Gatsouli, S. Pispas, E. I. Kamitsos and G. Floudas, *Macromolecules*, 48(2015)1473.
28. H. Song, N. Zhao, W. Qin, B. Duan, X. Ding, X. Wen, P. Qiu and X. Ba, *J. Mater. Chem. A*, 3(2015)2128.
29. J. Sakuda, E. Hosono, M. Yoshio, T. Ichikawa, T. Matsumoto, H. Ohno, H. Zhou and T. Kato, *Adv. Funct. Mater.*, 25(2015)1206.
30. P. Deshmukh, M. Gopinadhan, Y. Choo, S.-k. Ahn, P. W. Majewski, S. Y. Yoon, O. Bakajin, M. Elimelech, C. O. Osuji and R. M. Kasi, *ACS Macro. Letters*, 3(2014)462.
31. L. D. McIntosh, M. W. Schulze, M. T. Irwin, M. A. Hillmyer and T. P. Lodge, *Macromolecules*, 48(2015)1418.
32. Y. Tong, L. Chen, Y. Chen and X. He, *Appl. Surf. Sci.*, 258(2012)10095.
33. G. Adam and J. H. Gibbs, *J. Chem. Phys.*, 43(1965)139.
34. N. A. Stolwijk, M. Wiencierz, C. Heddier and J. Kösters, *J. Phys. Chem. B*, 116 (2012) 3065
35. H.-Y. Wu, D. Saikia b , C. Lin, F. Wu , G. T.K. Fey and H. Kao, *Polymer*, 51 (2010) 4351

36. J. R. Nair, M. Destro, F. Bella, G. B. Appetecchi and C. Gerbaldi, *J. Power Sources*, 306 (2016) 258
37. Q. Wang, W.-L. Song, L.-Z. Fan and Y. Song, *J. Membr. Sci.*, 486(2015)21.
38. L. Chen, Y. Li , S. Li, L. Fan, C. Nan and J. B. Goodenough, *Nano Energy*, 46 (2018) 176
39. I. Aldalur, H. Zhang, M. Piszcz, U. Oteo, L. M. Rodriguez-Martinez, D. Shanmukaraj and T. Rojo, M. Armand, *J. Power Sources*, 347 (2017) 37.

© 2020 The Authors. Published by ESG (www.electrochemsci.org). This article is an open access article distributed under the terms and conditions of the Creative Commons Attribution license (<http://creativecommons.org/licenses/by/4.0/>).